Yu Zhang
DongQin Li
Shihuan Hong
Miao Zhang

http://dx.doi.org/10.21278/brod74108

ISSN 0007-215X
eISSN 1845-5859

Design of a new oscillating-buoy type wave energy converter and numerical study on its hydrodynamic performance

UDC 551.46.09:681.883.065
Original scientific paper

Summary

In this study, with respect to wave energy generation technology, a new scheme is proposed for oscillating-buoy type wave energy conversion. A three-dimensional model of a power generation device is established based on SolidWorks, and a three-dimensional viscous numerical pool is setup using STAR-CCM+ to facilitate the simulation analysis of the device. The hydrodynamic performance and energy capture characteristics of the device were examined using theoretical analysis and numerical simulations. The regularities of parameters, such as motion response, force, and output power of the device, were analysed under four wave environments with different time periods (T) and wave heights (H). The analysis and conclusions can be utilised as a reference for studying the hydrodynamic performance of wave power generation devices.

***Key words**: Wave energy generation; Oscillating-buoy type; Computational fluid dynamics*

1. Introduction

In recent years, the exhaustion of fossil fuel resources, environmental problems, and growing energy demands have prompted active studies on the production of electricity from renewable energy sources. Among renewable energies, ocean wave energy has attracted increasing attention because of its high availability and low environmental impact [1]. Additionally, the energy density of ocean wave energy is significantly higher than that of solar energy, and it is more stable than wind energy [2, 3]. To date, several wave energy converter (WEC) concepts have been examined, and research has mainly focused on the mechanical structure, hydrodynamic aspect, and energy conversion rate of different WECs [4–7].

An oscillating buoy type wave energy converter is a type of wave energy converter (WEC). Its structural design and hydrodynamic performance can significantly impact the analysis of the motion characteristics and efficiency of wave energy generators. Researchers in Norway designed a power generator with a buoy as a sphere [8], which consists of a buoy and an upright column. Under the influence of the wave force, the buoy and column undergo relative motion and generate mechanical energy, which is then converted into electrical energy via a generator. Given that a single buoy energy generation device cannot effectively overcome the

effect of tidal differences, Irish scholars developed a wave energy generation device termed as Wavebob [9]. The device has two coaxial floaters with a rigid connection between the buoy and pontoon. The ingenious feature of this device is that it can be adjusted according to the wave frequency to match the incident wave frequency and realize the maximum efficiency of energy capture.

However, traditional buoy-type wave energy converters use an intermediate energy transfer system to convert wave energy into mechanical energy, and complex energy conversion can lead to low power generation efficiency. Therefore, it is essential to reduce the intermediate conversion link to improve the device efficiency. In recent years, Yue et al. [10] designed a Lysekil wave energy conversion device that can be directly driven with a direct connection between the buoy and generator. This in turn reduced the energy loss in the intermediate transmission link.

In this study, we propose to further simplify the structure and energy conversion process of an existing oscillating float device based on the research. A new type of oscillating float wave energy generation device is designed, and its hydrodynamic performance and energy capture characteristics are examined using theoretical analysis and numerical simulation. The analysis and conclusions provide a technical basis and reference for the engineering application of oscillating float wave power generation devices.

2. Design and energy conversion mechanism of a new oscillating float type wave energy generation device

2.1. Device design ideas and overall design

A three-dimensional model of a new oscillating float-type wave energy generation device is shown in Fig. 1. The design of the new device is fully based on the working mechanism of a traditional cylindrical oscillating float and Wells turbine [11-13], which can adapt to bidirectional airflow impact and maintain unidirectional rotation. By combining the two designs, it is possible to create torque via the unidirectional rotation of the blades during the lifting and sinking motions, which ultimately drive the generator to generate electricity.

A catenary mooring cable is used to hold the device in water, with one end attached to the bottom of the device and other end attached to a submarine base. Four damping plates are vertically assembled on a sleeve to maintain the overall vertical state of the device and to reduce the influence of the device tilt on power generation efficiency. The damping plate does not contribute to the overall energy transfer of the device. A generator system is an important part of a wave energy conversion device, and its generation characteristics and efficiency matching significantly influence device performance. The motor should have small rotor inertia and copper loss, and its starting torque should be relatively low. This device uses a permanent magnet brushless DC motor as power generation equipment. The vortex fan is the core part of the energy conversion device, which is also a structural innovation that differs from other wave energy conversion devices. Therefore, in this study, the wave energy absorber is considered as the key research object, and its hydrodynamic and power efficiency characteristics are systematically examined.

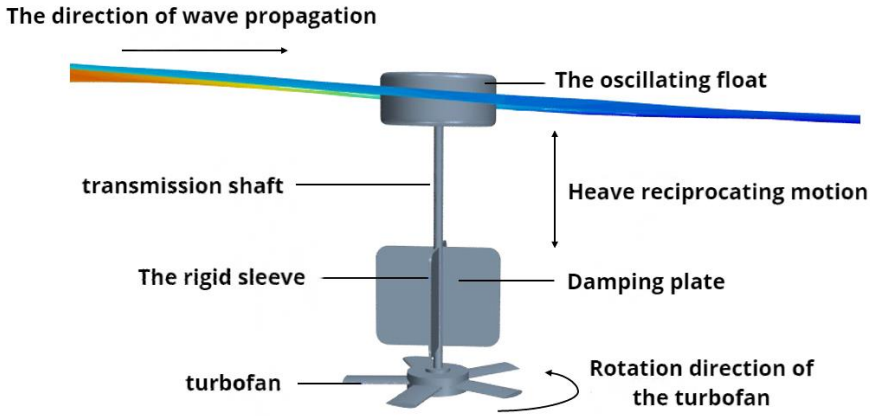

Fig. 1 New wave energy generation device

The longitudinal length of the device is 0.59 m and its total mass is 1.6837 kg, where the float diameter is 0.18 m and height is 0.12 m. The damping plate height is 0.16 m and width is 0.1 m. Turbofan blades are selected based on NACA0015 symmetrical wing type [14], and their specific parameters are listed in Table 1.

Table 1 Main parameters of the turbofan model

Wing type	NACA0015
Number of blades	5
Chord length (m)	0.05
Hub radius (m)	0.05
Radius of wheel rim (m)	0.15

2.2. Theoretical analysis of the energy conversion characteristics of the device

The energy-conversion process of the device is shown in Fig. 2, where energy is transferred in one direction during the transfer process.

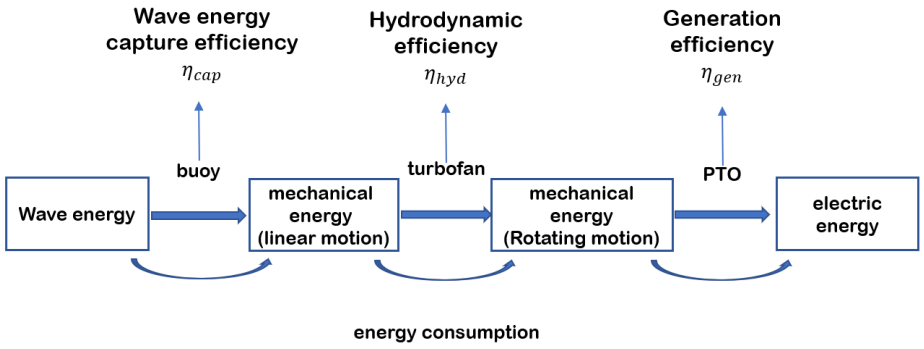

Fig. 2 Energy conversion process of the device

Overall efficiency η:

$$\eta = \eta_{cap} \cdot \eta_{hyd} \cdot \eta_{gen} \tag{1}$$

Turbofan input power P_{input}:

$$P_{input} = \frac{E_{input}}{t} = \frac{\frac{1}{2}\rho(\pi R^2)hV_A^2}{t} = \frac{1}{2}\rho\pi R^2 V_A^3 \quad (2)$$

E_{input} is the kinetic energy of a cylindrical fluid of height h and radius R that passes through the horizontal section of the fan blade at time t.

V_A denotes the relative flow rate between the fluid and horizontal cross section of the turbofan.

Output power of the turbofan P_{output} is as follows:

$$P_{output} = T\omega = NT_s\omega \quad (3)$$

where T denotes the output torque of the turbofan, ω denotes the rotation speed (rad⁄s), N denotes the number of blades of the turbofan, and T_s denotes the torque produced by a single blade on the drive shaft.

The generator power of a wave-energy generator P is as follows:

$$P = \eta \cdot C_l \cdot \dot{x}^2 \quad (4)$$

C_l denotes the linear damping coefficient of the wave energy-generating device, and x denotes the vertical displacement of the device.

According to a previous study [15], the rotational damping coefficient of generator C_r can be expressed as follows:

$$C_r = \frac{1.5K_r^2}{R_1+R_2} \quad (5)$$

where K_r denotes the torque constant of the generator, R_1 denotes the generator resistance, and R_2 denotes the external resistance of the circuit.

Furthermore, C_l can be expressed as follows:

$$C_l = \frac{1.5K_r^2}{\eta(R_1+R_2)e^2} \quad (6)$$

where e denotes the slope of the nonlinear relationship between the device heave speed and rotating speed of the turbofan.

The damping factor of the device is selected as approximately 8 N·s/m. The linear damping coefficient is related to the external load. The effective value of the external load can be adjusted based on the characteristics of the sea waves to realize the best damping ratio and wave capture ratio.

3. CFD simulation settings

3.1. Wave creation and dissipation

In the calculation of STAR-CCM+, three-dimensional, k–ω, Eulerian polynomial flow, implicit indeterminacy, and VOF wave models are selected.

In this study, a Stokes fifth-order wave is selected using the boundary condition wave-making method. The waves satisfy the following conditions at the boundary.

Velocity in x-direction:

$$u_x = c\sum_{n=1}^{5} n\,\lambda_n cosh[nk(z+d)] \times cos[n(kx-\omega t)] \quad (7)$$

Velocity in z-direction:

$$u_z = c\sum_{n=1}^{5} n\,\lambda_n sinh[nk(z+d)] \times sin[n(kx-\omega t)] \quad (8)$$

Instantaneous rise height of wave surface:

$$\eta = \frac{1}{k}\sum_{n=1}^{5}\lambda_n \cos[n(kx-\omega t)] \tag{9}$$

In the formula: ω, d, k denote circle frequency, water depth, and wave number, respectively, and the remaining coefficients are reported in previous studies [16].

A wave probe is setup to monitor the time course of the wave surface variation at different periods as shown in Fig. 3. It can be observed that the waves simulated in this study are in basic agreement with the fifth-order Stokes wave.

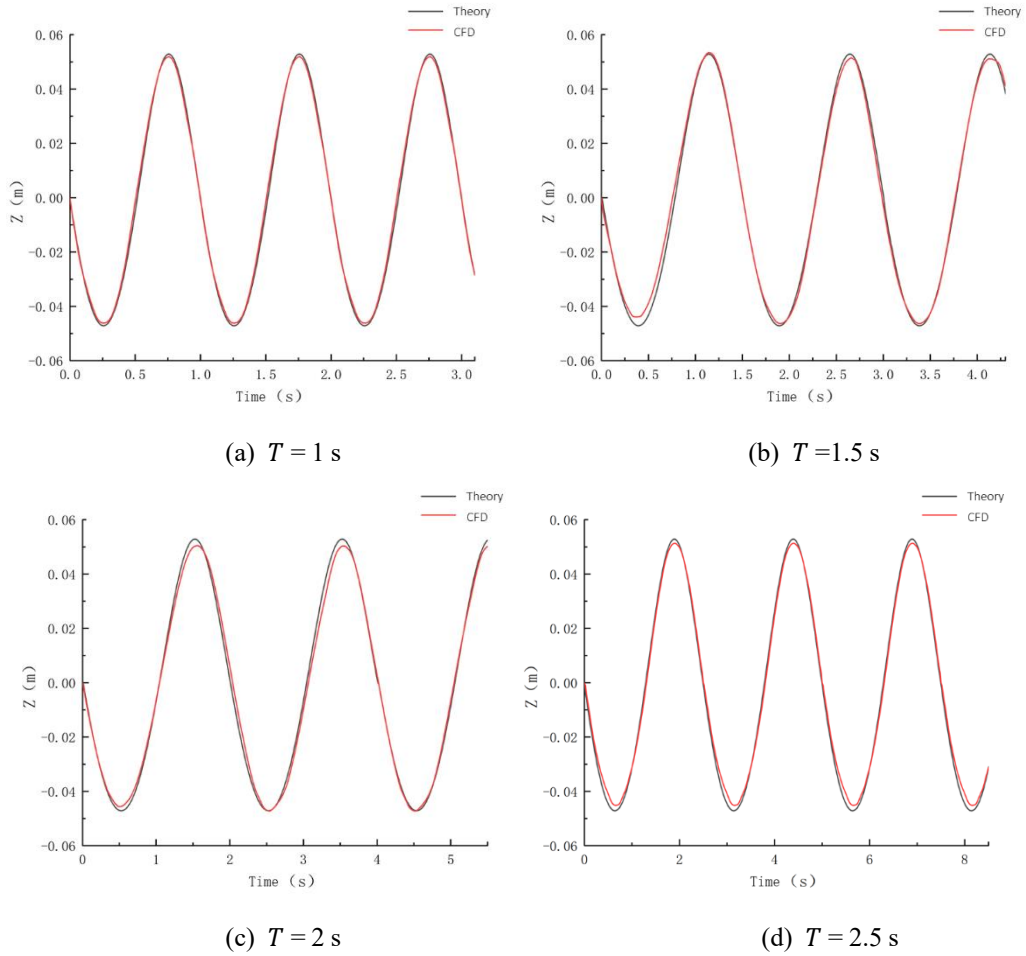

(a) T = 1 s (b) T =1.5 s

(c) T = 2 s (d) T = 2.5 s

Fig.3 Time history curve of wave height at each wavelength monitoring point

Wave annihilation refers to the setup of a wave dissipation zone in the outlet area of a numerical pool to prevent wave reflection from affecting the waveform and calculations in the calculation area. In this study, a damping absorber [17] is used to set a distance of length λ at the outlet end of the pool as a damping absorber zone.

3.2. Computational domain and mesh generation

The computational domain is set based on the wave wavelength when wave period T = 1.5 s. The entrance boundary is located in the negative direction of the x-axis at a distance of 1λ from the origin, and the exit boundary is located in the positive direction of x-axis at a distance of 2λ from the origin, with a total length of 3λ. The computational domain is 2.56 m wide and 2.08 m high, with a water depth of 1 m and 1.08 m above the water surface, and it is encrypted near the water surface, in the background, and in the motion overlap area with a total

of approximately 1 million computational grids [18–19]. The computational domain setup is illustrated in Fig. 4.

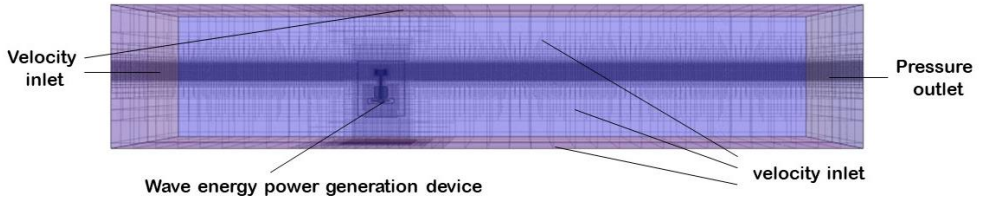

Fig. 4 Computational domain setup and meshing

3.3. Independence verification

Independence testing ensures that the accuracy and convergence of the CFD analysis are not affected by software settings. To ensure the accuracy of the output results of the numerical simulation, computational resources are saved and computational efficiency is improved. Setting parameters, such as mesh size and maximum iteration times of each time step, significantly influences the numerical simulation of the hydrodynamic characteristics of the device. A reasonable selection of parameters can ensure calculation accuracy and accelerate research. In this study, the device is selected as the analysis object when $T = 1.5$ s and $H = 0.1$ m, and the change law of the blade rotation velocity increases and decreases with the aforementioned parameters.

Figure 5 shows the grid number independence curve. An increase in the number of grids implies that the grid size is relatively reduced. Hence, the grid division in the field of power generation equipment computing is more refined. It can be observed that the rotation velocity of the fan increases with an increase in the number of grids and tends to be stable at approximately 1 million. Therefore, in the numerical simulation of the wave power generation device used in this study, a grid number of 1 million is appropriate.

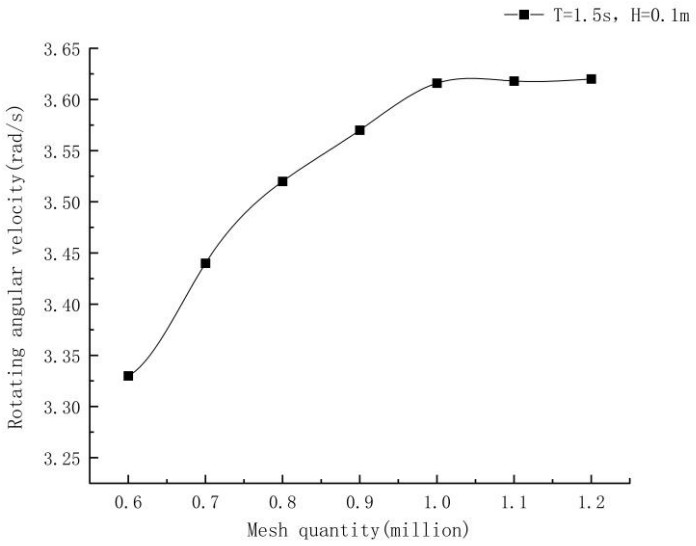

Fig. 5 Independent test curve of the number of grids

In the calculation of fluid instability, the maximum number of iterations for each time step significantly influences the calculation result. Excessive iteration times increase the occupation

of computing resources and do not improve computing accuracy. Figure 6 shows the independence curve of the maximum number of iterations per step. It can be observed that the turbofan speed decreases with an increase in the maximum number of iterations and tends to become stable at 20 iterations per step. Therefore, the maximum number of iterations of each time step should be set to 20 in the numerical simulation of the hydrodynamic characteristics of the power generation unit in this study. Based on an independent test of the number of grids and maximum iteration times of the time steps, it is reasonable to select the number of grids and maximum iteration times as 1 million and 20, respectively, for the numerical simulation of the power generation plant.

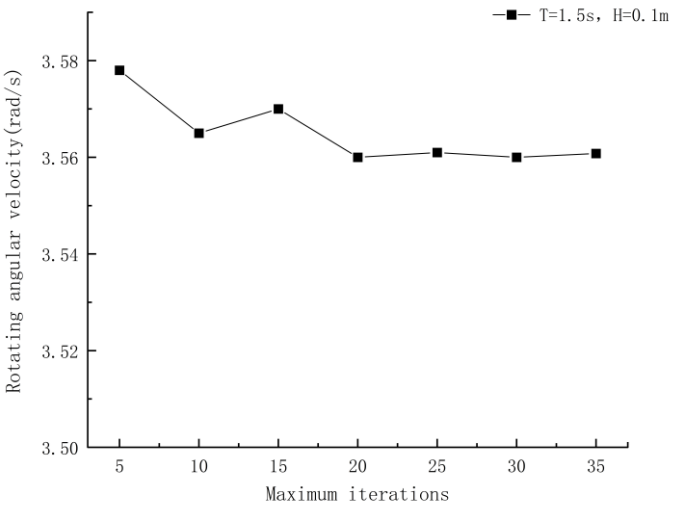

Fig. 6 Independent test curve of the maximum number of iterations per time step

4. Numerical calculation and analysis of results

In this study, four types of waves with different periods and wave heights are selected for the calculation to analyse the force, motion response, and output power of the device.

4.1. Hydrodynamic performance analysis of the device within one wavelength

The damping plate of the new power generator is not involved in the transfer of energy but only serves to maintain the stability of the device in water. In the CFD simulation, the device is in a state where all six degrees of freedom are released. The energy is acquired in the heave direction of the oscillating float. If the device deviates in the horizontal direction due to rolling, pitching, and surge, then these conditions affect the power generation performance of the device. Therefore, the stability of the device is first analysed. In the simulation, the rotating centre of the turbofan is considered as the monitoring point, and the *Z*-axis is considered as the reference axis. Given that the positive direction of *X* is the direction of the wave flow and the device offset distance in the *Y* direction is small in both cases, the displacement of the monitoring point in the *X* direction in both cases is analysed. The details are shown in Fig. 7.

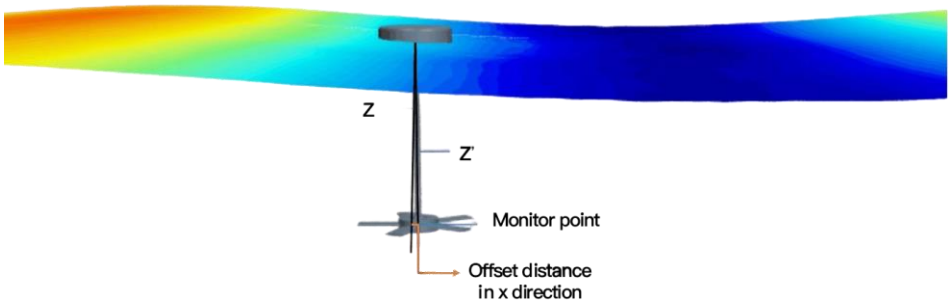

Fig. 7 *X* direction offset of devices without damping plates in waves

A comparison after the damping plate is installed is shown in the figure below. Figure 8 shows that the device migration period is the same as the wave cycle with a maximum deviation of up to 0.16 m and total deviation of approximately 0.3 m. After the damping plate is installed, the total deviation amplitude of the device is approximately 0.007 m, which improves its stability.

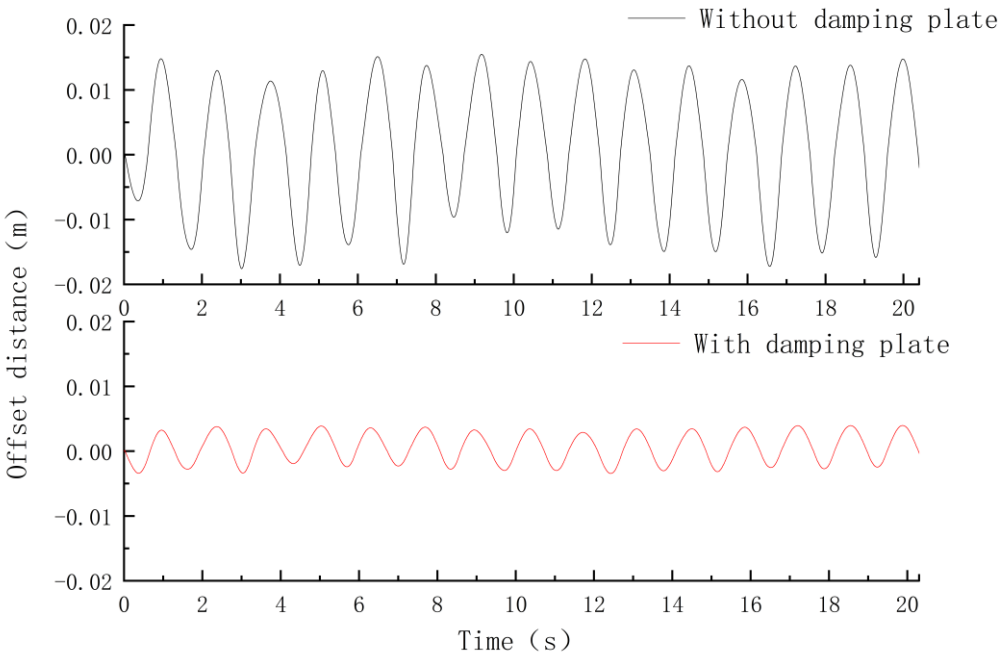

Fig. 8 Comparison of the X direction shift of the device in the waves

To visualise the motion of the floating body at different times, the motion of the device at a wave height of H=0.1 m and period T=1.5 s is shown in Fig. 9.

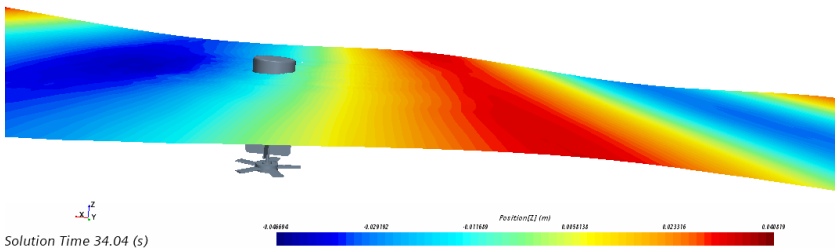

(a) $t = 34.04$ s

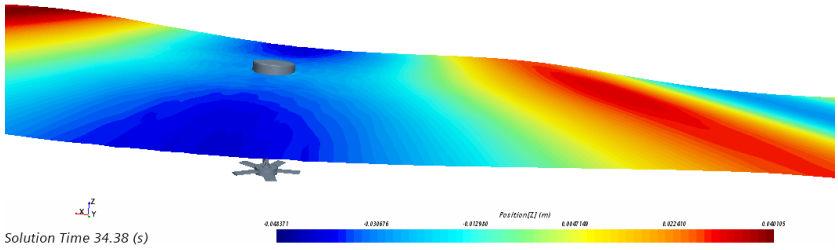

(b) $t = 34.38$ s

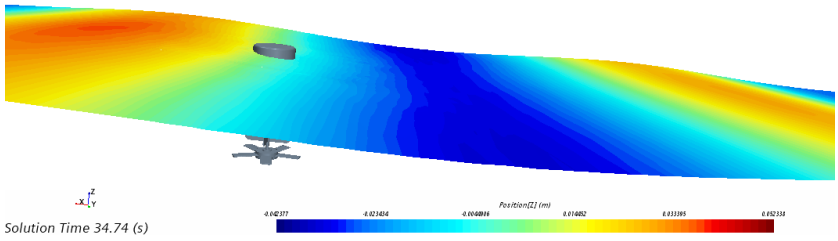

(c) $t = 34.74$ s

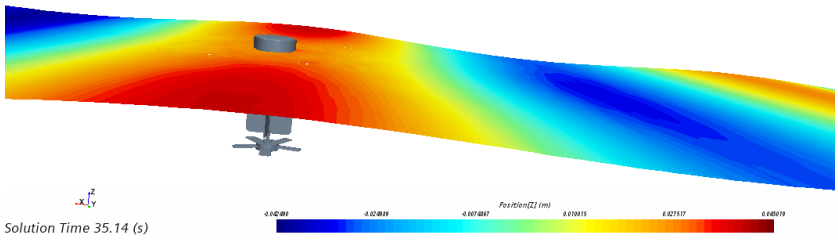

(d) $t = 35.14$ s

Fig. 9 $T = 1.5$ s, $H = 0.1$ m diagram of the motion of the power generator in one λ

Figures 9 and 10 show that the device makes a vertical oscillation motion along the wave surface. Figure 9 (a) shows that the device just crosses a wave crest and moves downward along the wave face when the vertical velocity along the opposite direction of the Z-axis is maximum, approximately −0.141 m/s. Figure 9 (b) shows that the device moves downward along the wave face to the trough, and the vertical velocity of the device is nearly 0. Figure 9 (c) shows that the floater moves upward along the wave face, and the device vertical velocity is maximum along the positive direction of the Z-axis at approximately 0.148 m/s. Figure 9 (d) shows that the floater reaches the wave crest, and the vertical displacement of the device reaches its maximum.

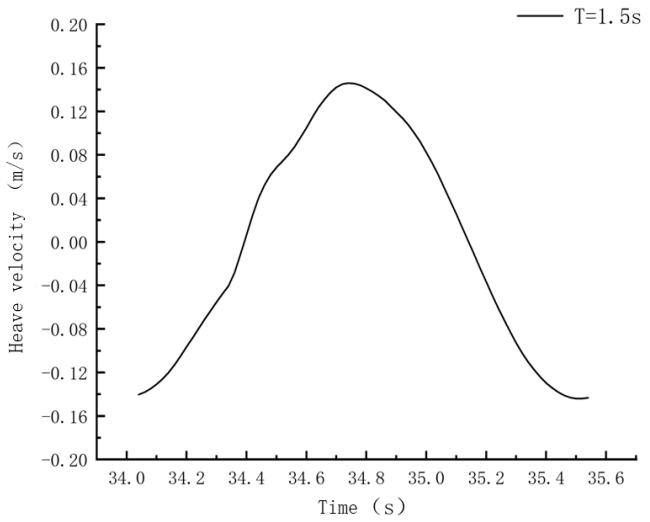

Fig. 10 Time history curve of device droop velocity

As shown in Fig. 10, the heave motion speed of the device changes periodically with the wave. When the device moves to the position of the free surface, it has a maximum dangling speed. When it is in the wave crest or wave trough position, it moves in the opposite direction because of the restoring force. The heave speed is approximately 0.

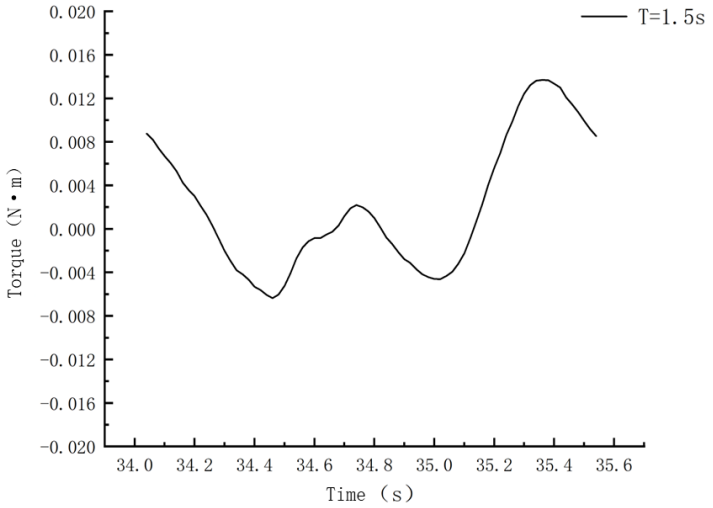

Fig. 11 Time history curve of fan blade torque

As shown in Fig. 11, the torque of the device under the influence of the wave experiences a periodic change. When t = 34.38 s, the trough of the fan, the reverse rotational torque of the fan blade is higher, approximately −0.0047 Nm. When t = 35.14 s, at the peak of the wave moment, the blade torque is 0 Nm. However, given the inertia of the turbofan, the blade continues to rotate when the rotation torque is 0 for the blade [20].

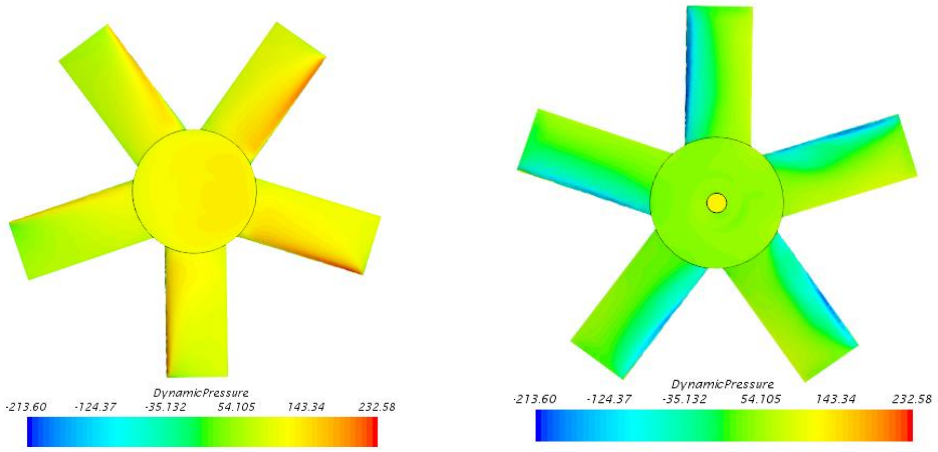

(a) Blade pressure side at $T = 1.5$ s (b) Blade suction side at $T = 1.5$ s

Fig. 12 Turbofan dynamic pressure cloud diagram at $T = 1.5$ s

Figure 12 shows a dynamic pressure cloud diagram of the turbofan. In this study, we define the direction of the vertical downward observation from the wave surface as the suction side of the blade and direction of upward observation from the bottom of the pool as the suction side of the blade. It can be observed that the high-pressure area of the blade is mainly concentrated in the front edge of the blade, and the maximum pressure difference is 446.18 Pa. The pressure on the pressure side of the blade is mainly positive, whereas the suction side is negative. The pressure difference on the blade surface gradually decreases along the chord length direction and approaches zero at the trailing edge. Therefore, the output torque of the turbofan is mainly provided by the pressure difference at the leading edge of the blades.

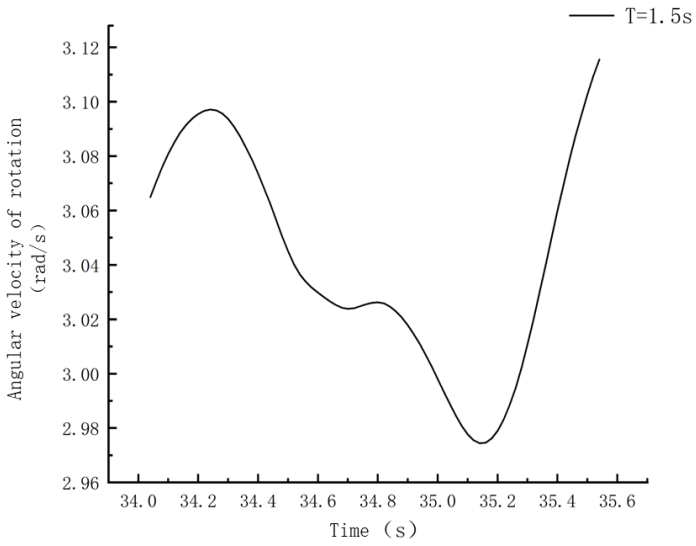

Fig. 13 Time history curve of fan blade rotation angular velocity

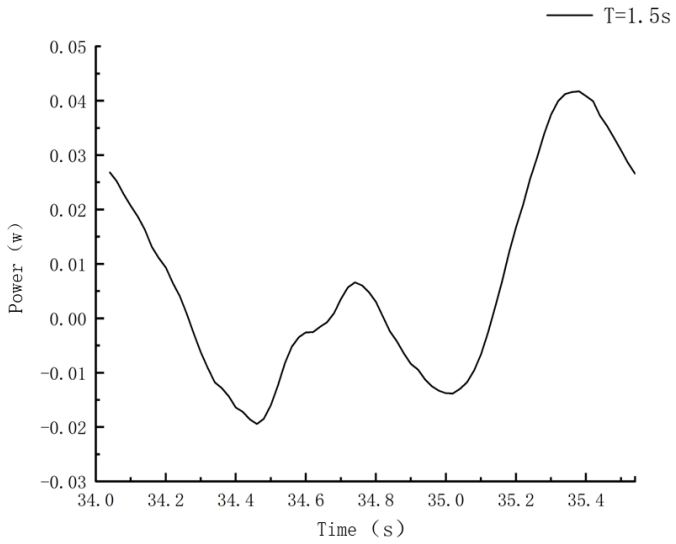

Fig. 14 Output power

Figure 13 shows that at 35.14 s when the buoy is in the peak position, the blade torque is 0 N·m. The turbofan continues to rotate because of inertia, and the angular velocity is the lowest at this time which is approximately 2.97 rad/s. The float is in the trough, and the angular speed of rotation is faster around 34.38 s. When the buoy rises from the trough to the peak, the rotational angular velocity decreases; however, when it decreases from the peak to trough position, the angular velocity increases significantly.

As shown in Fig. 14, the instantaneous power output of the turbofan varies within a wavelength range, and the variation pattern is roughly equivalent to that of the torque. At t = 34.38 s, the fan blade is subjected to a large reverse rotational torque. Hence, the instantaneous output power reaches the minimum value, which is approximately −0.014 W. At the peak time t = 35.14 s, the blade torque is 0 Nm, and the instantaneous output power is 0 W.

4.2. Effect of period time on the hydrodynamic performance of the device

In this section, the waves of the four periods are separately selected for analysis. The wave parameters are listed in Table 2. When the period is less than 1 s, the wave attenuates significantly owing to the viscous effect. Therefore, waves with a period of more than 1 s are selected for simulation in this study. The numerical wave pool is developed by referring to the physical experiments and numerical simulation of wave energy power generation devices designed by Wang Di of Shanghai Jiao Tong University and similar devices reported in previous studies [21-22]. The selected wave parameters are listed in Table 2.

Table 2 Wave parameters at different periods

Work conditions	Periodicity T (s)	Pogo H (m)	Wavelength λ (m)
W_1	1	0.1	1.6199
W_2	1.5	0.1	3.3789
W_3	2	0.1	5.2371
W_4	2.5	0.1	7.0124

The motion of the device in the wave is mainly analysed in the following aspects: the

overall device motion speed in the direction of the pendulum, displacement, blade torque, turbofan rotation angular velocity, dynamic pressure, and output power.

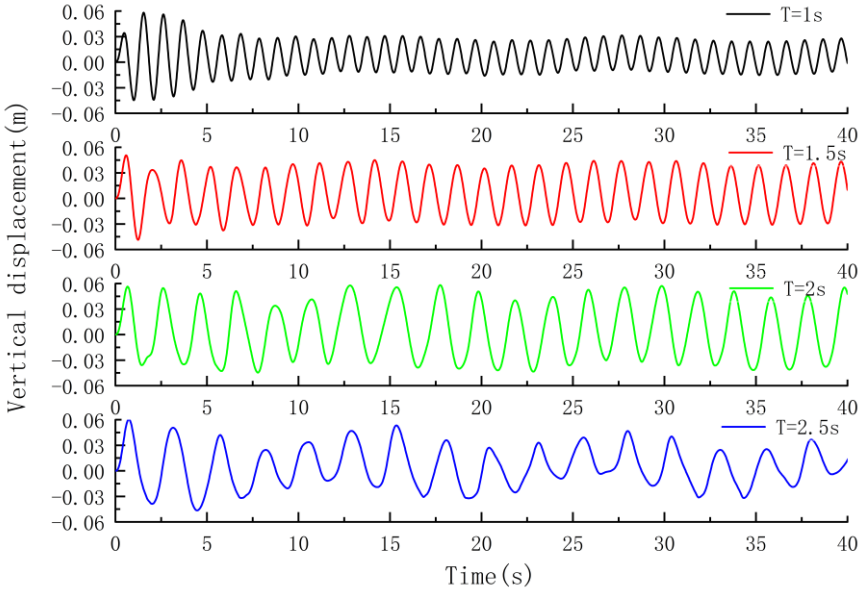

(a) Vertical displacement

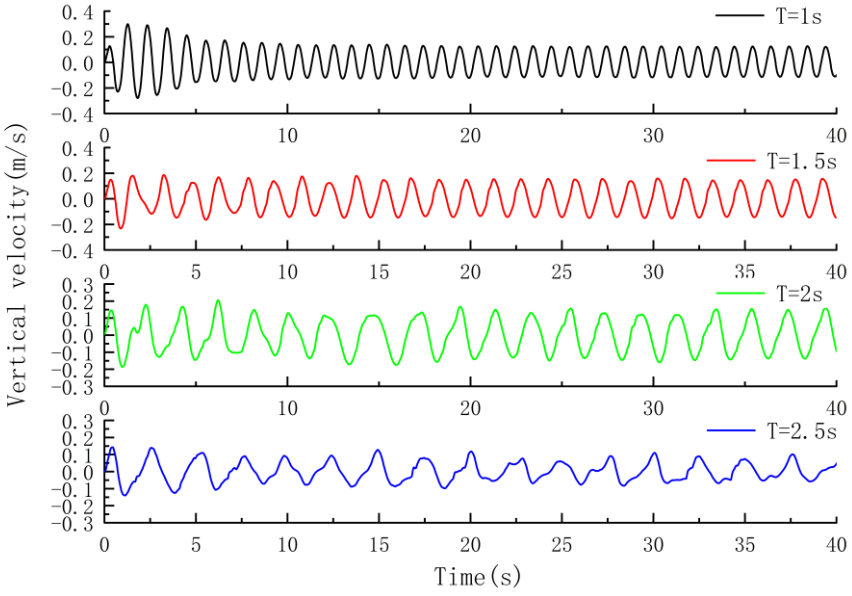

(b) Vertical velocity

Fig. 15 Time history curves of vertical displacement and velocity at different periods

At T = 1 s, the wave propagation frequency increases owing to the shortest wavelength, making the initial vertical velocity of the device greater than that for the other periods. At T = 2.5 s, the wavelength becomes longer and device vertical response velocity becomes smaller. This is due to the fact that the wave input energy increases when the period increases, but the rate of change of the energy absorbed by the float is smaller than the rate of change of the incident wave input energy. Hence, the overall vertical velocity of the device is relatively low

[23]. When the displacement tends to change in a stable pattern, it can be obtained at $T = 2$ s, and the device vertical displacement amplitude is the highest at approximately 0.09 m. At $T = 1$ s, the vertical displacement amplitude is the lowest at approximately 0.04 m. It can be observed that the dynamic response of the float system is more evident during small periods (high wave frequency), which implies that the number of vibrations per unit time of the combined vertical force of the device increases as the incident wave period decreases, and the number of float vibrations is inversely proportional to the incident wave period.

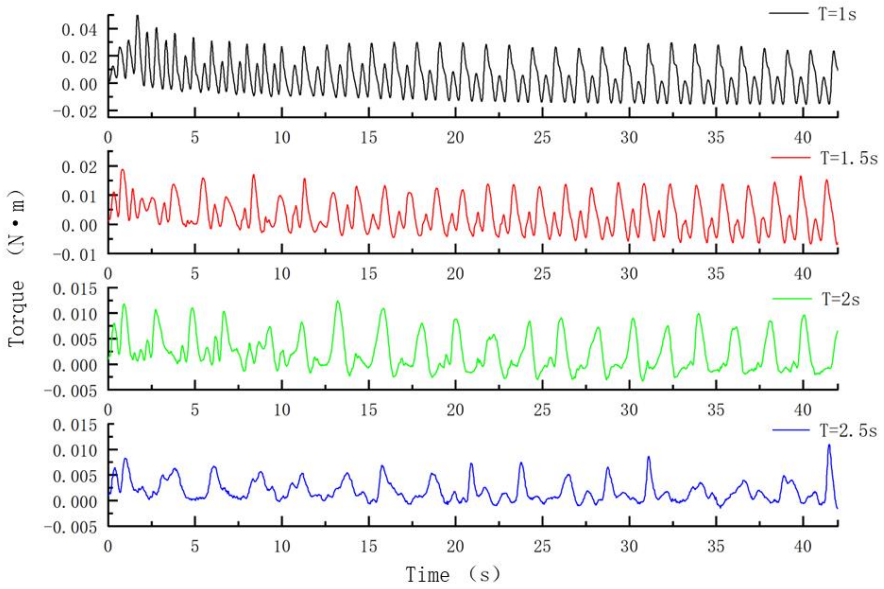

Fig. 16 Time history curve of fan blade torque at different periods

The time-history curve of the turbofan blade torque is shown in Fig. 16. The blade torque varies periodically under the influence of waves, and the rotational torque is influenced by the wave period. The torque at wave period of $T = 1$ s is the maximum when compared with other periods, and the maximum torque amplitude is approximately 0.025 Nm. Furthermore, the minimum torque amplitude is at wave period of $T = 2.5$ s, and the minimum torque amplitude is approximately 0.006 Nm. The blade torque decreases with increasing wave period.

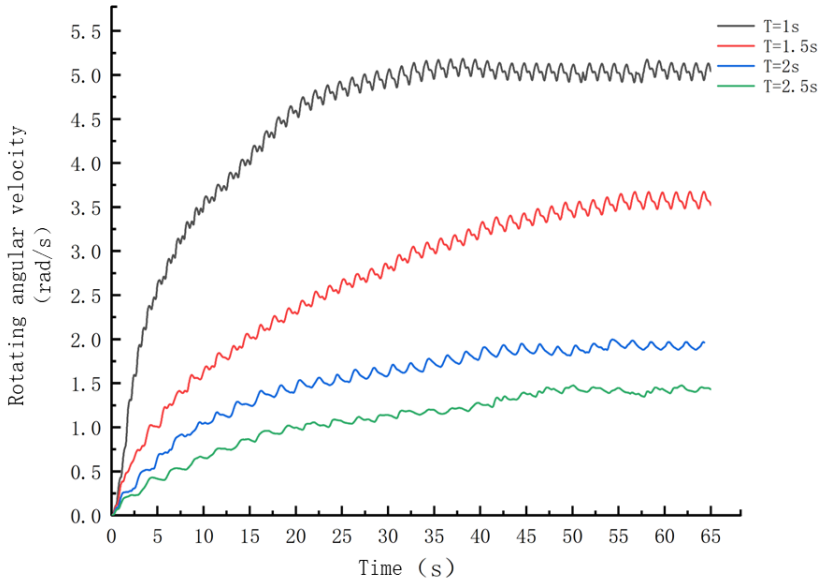

Fig. 17 Time history curve of blade rotation speed at different periods

The time-history curve of the turbofan angular velocity is shown in Fig. 17. From Fig. 17, it can be observed that the angular velocity of the turbofan rotation increases gradually with time, and after a period of time, it converges to stability. At $T = 1$ s, the turbofan speed converges to 4.98 rad/s, which is the maximum constant speed. At $T = 2.5$ s, the turbofan speed converges to approximately 1.41 rad/s, and the speed is the lowest. It can be observed that with a gradual decrease in the wave period, the turbofan speed gradually increases.

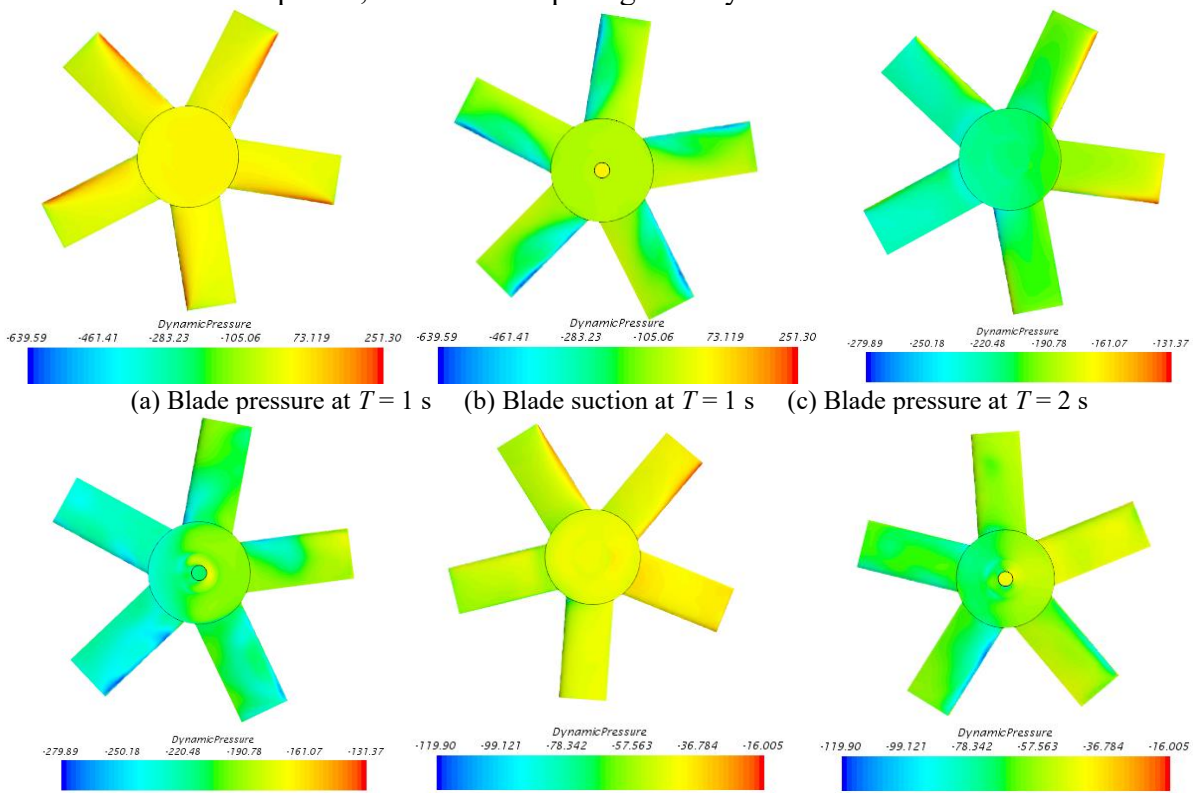

(a) Blade pressure at $T = 1$ s (b) Blade suction at $T = 1$ s (c) Blade pressure at $T = 2$ s

(d) Blade suction side at $T = 2$ s (e) Blade pressure side at $T = 2.5$ s (f) Blade suction side at $T = 2.5$ s

Fig. 18 Turbofan dynamic pressure cloud at different periods

By comparing the dynamic pressure cloud in Fig. 18, it can be observed that the blade pressure distribution law is similar. Specifically, the high-pressure area of the blade is mainly concentrated on the leading edge of the blade, and the pressure difference on the blade surface gradually decreases along the chord length direction and tends to zero at the trailing edge. At $T = 1$ s, the maximum pressure difference of the blade is 890.89 Pa. At $T = 2$ s, the maximum pressure difference of the blade is 411.26 Pa. At $T = 2.5$ s, the maximum pressure difference of the blade is 148.82 Pa. The pressure difference at the leading edge of the blade surface gradually decreases with an increase in the wave period T. This implies that the appropriate reduction in wavelength can increase the pressure difference between the two sides of the blade leading edge, expand the high-pressure difference area, and then increase the rotational torque of the turbofan.

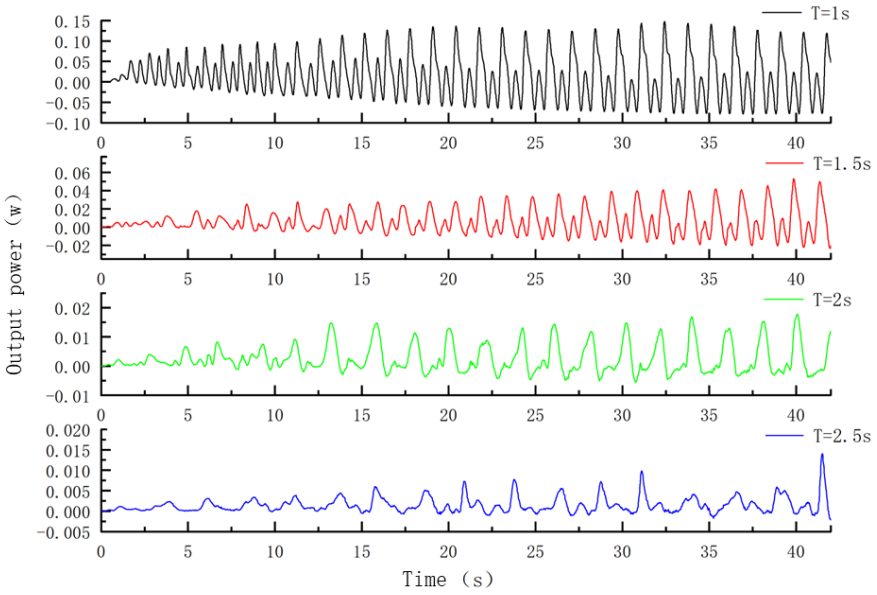

Fig. 19 Output power at different periods

The instantaneous output power curve of the device is shown in Fig. 19. It can be observed that the output power of the power generation device approaches a stable amplitude after a period of time in all four wave period environments. When $T = 1$ s, the maximum instantaneous output power of the turbofan is 0.122 W, and the lowest output power is at $T = 2.5$ s. Combining $T = 1.5$ s and $T = 2$ s shows that the instantaneous power output of the device decreases with increasing period. This is due to the fact that the relative speed between the wave and turbofan decreases with increasing period, and the output power is proportional to the blade rotation speed, which decreases the output power.

Table 3 Comparison of calculation results under different cycles

Working condition	Pendular displacement amplitude (m)	Pendulum velocity amplitude (m/s)	Rotational torque amplitude (N·m)	Rotation speed (rad/s)	Maximum instantaneous power （W）
W_1	0.027	0.12	0.025	4.98	0.122
W_2	0.042	0.15	0.015	3.57	0.053
W_3	0.045	0.13	0.008	1.93	0.016
W_4	0.036	0.08	0.006	1.41	0.008

As listed in Table 3, when $T = 1.5$ s, the device droop velocity amplitude is higher and corresponds to 0.15 m/s. At $T = 1$ s, the device droop displacement amplitude is the lowest (0.027 m), but the output power is the highest. This is due to the increase in wavelength. Specifically, the nonlinear effect owing to the change in wave steepness decreases, whereas the nonlinear effect due to the relative wave height and relative water depth increases, and thereby, more energy is lost when the wave interacts with the device. Therefore, an appropriate adjustment of the period can enhance the output power of the device. However, in practical engineering, this period cannot be indefinitely reduced. This is due to the fact that it causes the power generation device to vibrate too fast and easily causes energy shock and waste. Furthermore, it poses difficult challenges to the working performance of the related supporting power generation system [24–26].

4.3. Effect of wave height on the hydrodynamic performance of the device

After complete examination of the effects of wave conditions of different periods on the hydrodynamic performance of the power generation device, a specific wave period of T = 1.5 s is selected, in this section, to analyse the motion response and power generation of the device under different wave height parameters. The selected wave parameters are presented in Table 4.

Table 4 Wave parameters at different wave heights

Working condition	Period T (s)	Wave height H (m)	Wavelength λ (m)
A_1	1.5	0.05	3.3789
A_2	1.5	0.1	3.3789
A_3	1.5	0.15	3.3789
A_4	1.5	0.2	3.3789

As shown in Fig. 20, the device exhibits a periodic variation in the vertical oscillation displacement and velocity under the wave influence of different wave heights. Given that the wave conditions exhibit the same period and only the wave heights differ, a dimensionless T is introduced to describe the device response to wave motion, which is defined as the ratio of the vertical motion amplitude of the device to the wave height. In the figure, it can be observed that the vertical motion amplitude is 0.031 m at H = 0.05 m, 0.068 m at H = 0.1 m, 0.104 m at H = 0.15 m, and 0.117 m at H = 0.2 m, and the corresponding period T is 0.62, 0.68, 0.693, and 0.685, respectively. It can be observed that at H = 0.15 m, the device responds relatively well to the wave motion.

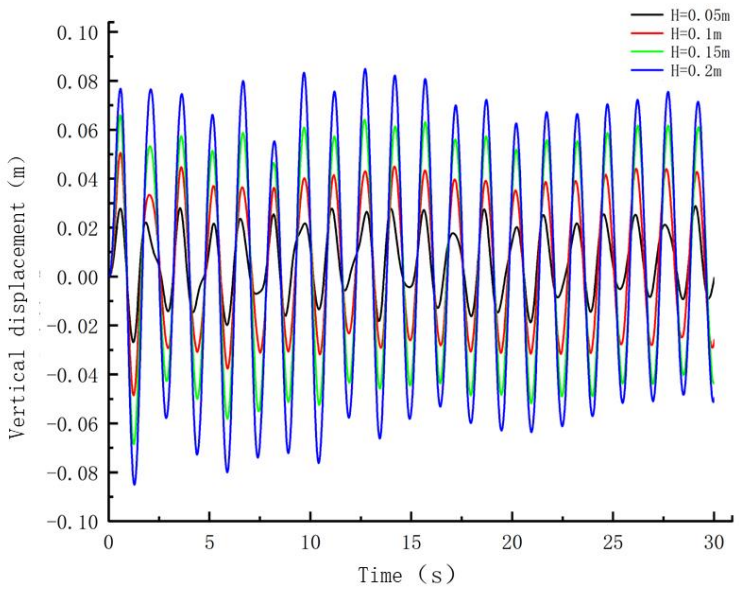

(a) Vertical displacement

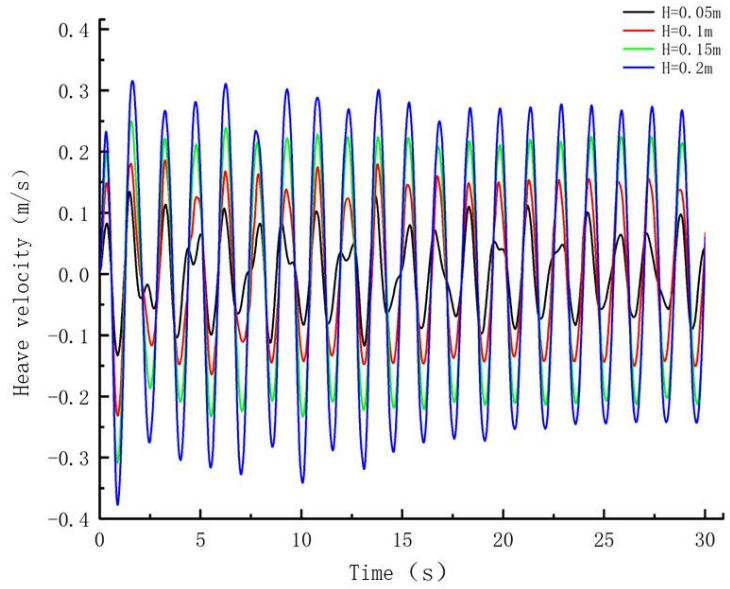

(b) Vertical velocity

Fig. 20 Time history curves of vertical displacement and velocity at different wave heights

Additionally, it can be observed that the device droop velocity exhibits periodic variation. When H = 0.2 m, the wave droop speed is the highest with an amplitude of 0.26 m/s. When H = 0.15 m, the wave droop speed is 0.22 m/s. When H = 0.05 m, the wave droop speed is the smallest with an amplitude of 0.08 m/s. A pattern can be obtained where the dip velocity of the device increases with the wave height for the same wave period.

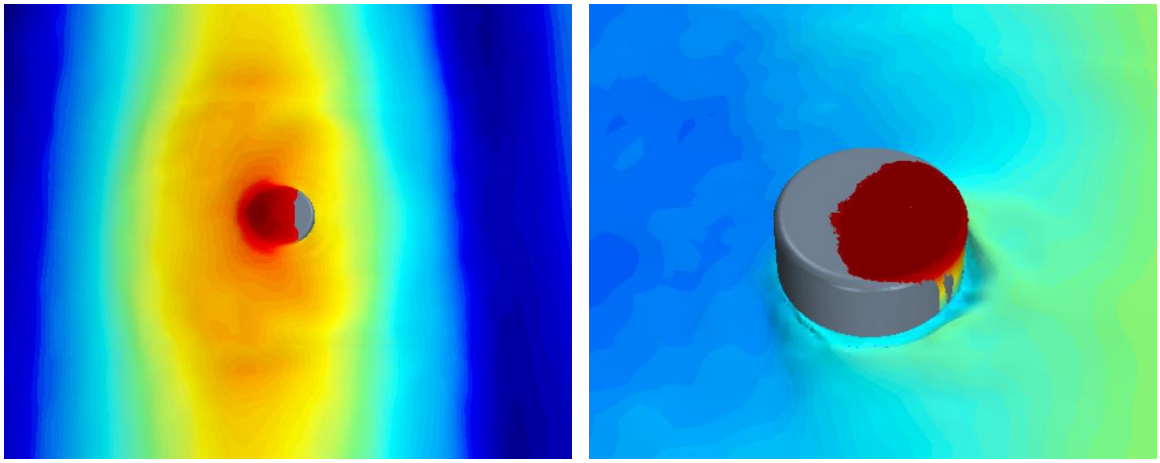

Fig. 21 *H*=0.02 m float on the wave

Figure 21 shows an upwelling situation of the buoy when *H*=0.02 m. Due to the fixed wavelength, *H*=0.02 m has relatively high wave amplitude, which leads to a steeper wave. Given that the relative motion amplitude between the hull and waves is high, seawater diffuses over the surface of the float for a period of time and eventually flows out of the surface. In this case, the device still operates normally; therefore, the upper waves do not cause significant damage under this wave parameter. Furthermore, the power generation device at other wave heights does not exhibit the upwelling phenomenon, thereby indicating a positive correlation between the upwelling load and wave amplitude or wave steepness.

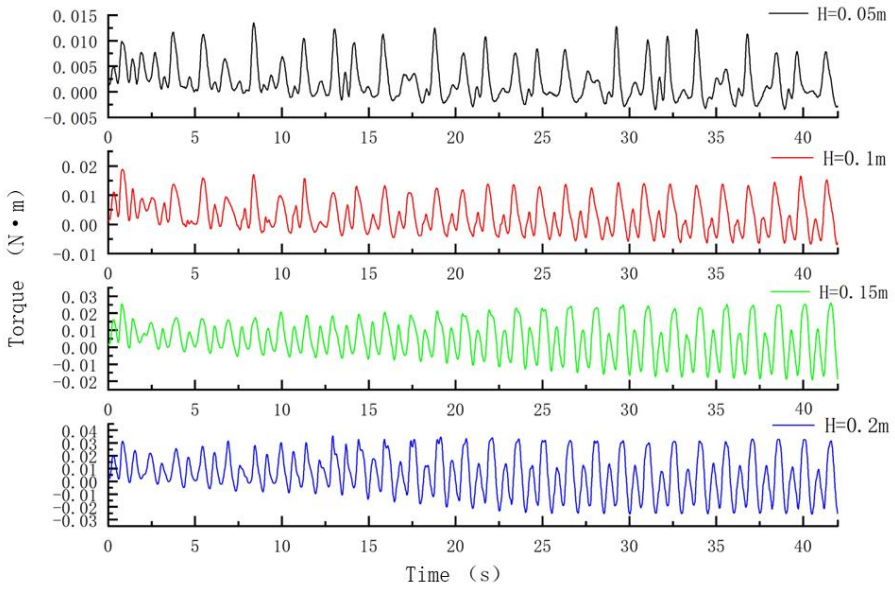

Fig. 22 Time history curve of fan blade torque at different wave heights

As shown in Fig. 22, the blade torque varies periodically under the influence of the wave, and the rotating torque is affected by the wave height. When the wave height is H = 0.2 m, the torque is maximum, and the maximum torque amplitude is approximately 0.032 Nm. When the wave height is H = 0.15 m, the fan blade torque amplitude is approximately 0.025 Nm. When the wave height is H = 0.05 m, the torque is minimum, and the minimum torque amplitude is approximately 0.008 Nm. The blade torque increases with wave height.

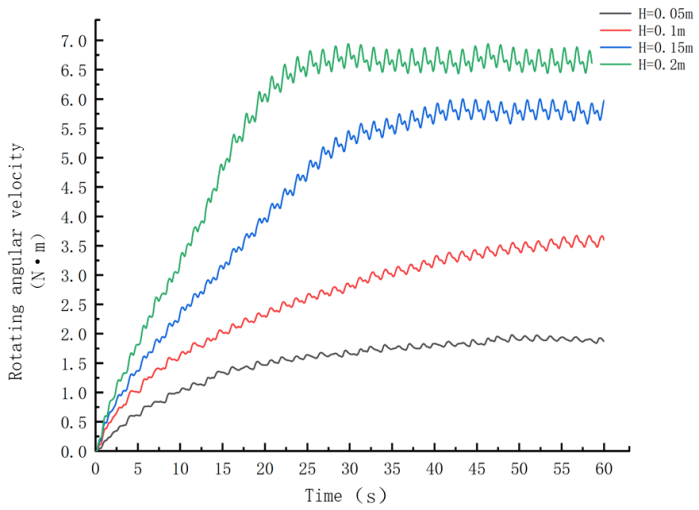

Fig. 23 Time history curve of blade rotation speed at different wave heights

The time-history curve of the turbofan angular velocity is shown in Fig. 23. When H = 0.05 m, the turbofan speed converges to 1.91 rad/s after a period of time, and the constant speed of the turbofan is the smallest in this wave environment. When H = 0.1 m, the turbofan speed converges steadily to approximately 3.57 rad/s. When H = 0.15 m, the turbofan speed converges steadily to approximately 3.57 rad/s. When H = 0.15 m, the turbofan speed converges to 5.78 rad/s. The turbofan speed converges to approximately 6.67 rad/s when H = 0.2 m. It can be observed that the turbofan speed increases gradually with a gradual increase in wave height.

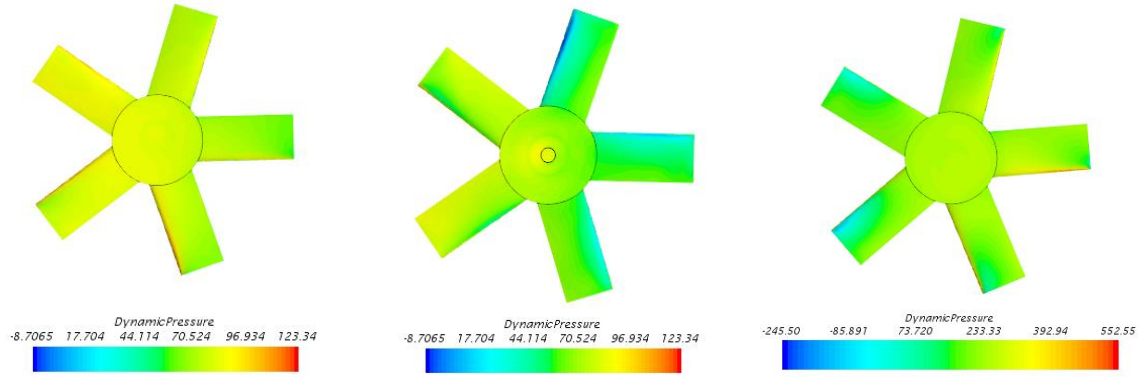

(a) Blade suction side at H = 0.05 m (b) Blade pressure side at H = 0.05 m (c) Blade pressure side at H = 0.15 m

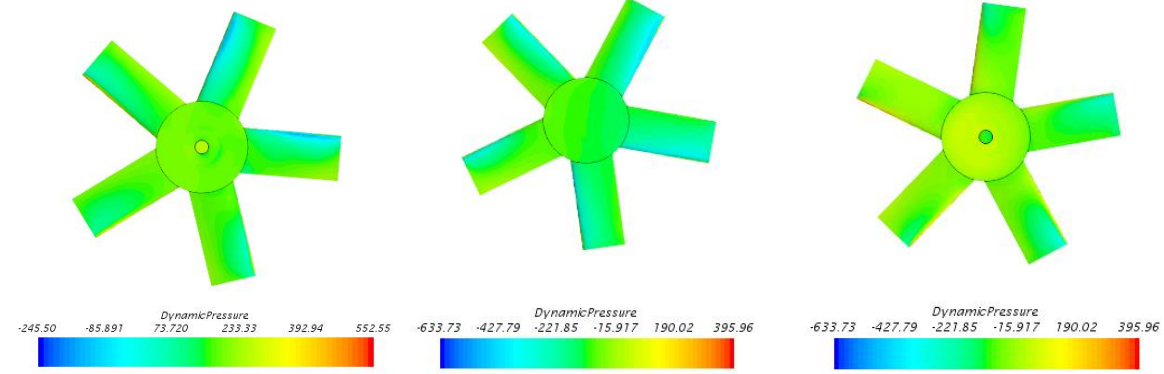

(d) Blade suction side at H = 0.15 m (e) Blade pressure side at H = 0.2 m (f) Blade suction side at H = 0.2 m

Fig. 24 Turbofan dynamic pressure cloud at different wave heights

Combined with the previous blade dynamic pressure cloud when $H = 0.1$ m and compared with Fig. 24, we can observe that the blade pressure distribution law under different wave heights is similar. When $H = 0.05$ m, the maximum pressure difference at the leading edge of the blade is 132.0465 Pa. When $H = 0.15$ m, the maximum pressure difference at the leading edge of the blade is 798.05 Pa. When $H = 0.2$ m, the maximum pressure difference at the leading edge of the blade is 1029.69 Pa. The pressure difference at the leading edge of the blade surface gradually increases with as wave height H increases. It can be observed that when the period is the same, an increase in the wave height can lead to an increase in the pressure difference on both sides of the leading edge of the blade, expand the high-pressure difference area, and then increase the rotating torque of the turbofan.

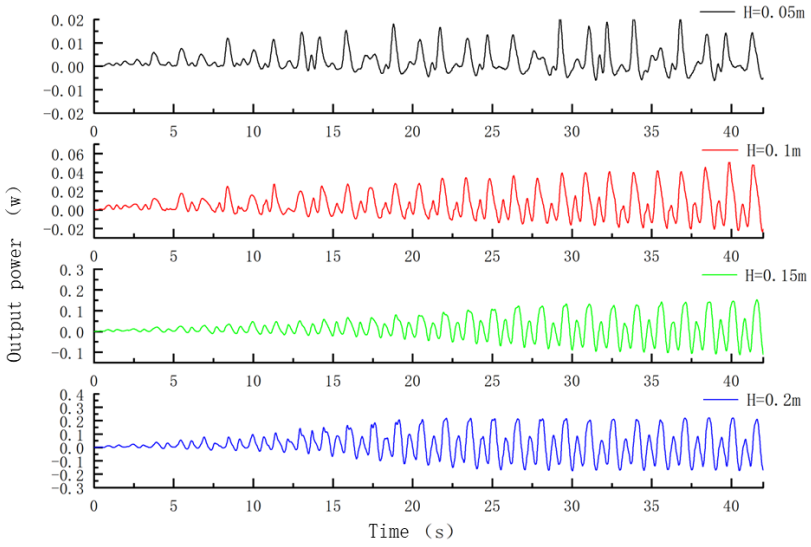

Fig. 25 Output power at different wave heights

As shown in Fig. 25, the instantaneous output power curve of the device indicates that the output power of the power generator tends to stabilise after a period of time. It is observed that the instantaneous output power increases as wave height increases. This is due to the fact that when the wave height period increases, the heave speed of the device and rotation speed of the turbofan increase accordingly. The output power is proportional to the rotation speed of the blade. Therefore, when the blade rotation angular speed increases, the output power increases accordingly.

Table 5 Comparison of calculation results under different wave heights

Working condition	Dimensionless T	Pendulum speed amplitude (m/s)	Rotational torque amplitude (Nm)	Rotational speed (rad/s)	Maximum instantaneous power（W）
A_1	0.62	0.08	0.008	1.91	0.016
A_2	0.68	0.15	0.015	3.57	0.053
A_3	0.693	0.22	0.025	5.78	0.142
A_4	0.685	0.26	0.032	6.67	0.211

As listed in Table 5, the amplitude of the device and wave motion exhibit best fit at

different wave heights when $H = 0.15$ m. Furthermore when $H = 0.2$ m, the device exhibits the fastest vertical motion. In this case, the turbofan rotation speed is the fastest, and the output power is the highest. This is due to the fact that when the wavelength is fixed, the non-linear effect owing to the wave height and water depth change is enhanced, and appropriate adjustment of the wave height aids in increasing the output power of the device. However, the wave height cannot be increased indefinitely, which leads to extremely steep waves and upwelling [27]. There are three potential reasons for the rising waves: the unreasonable arrangement of the power generation device, underestimation of the design value of the float elevation, and extremely high actual wave crest, which further enhances the nonlinear phenomenon caused by it. In this study, it is verified that the first two causes are excluded, and the hydrodynamic performance of the device and feasibility of power generation are analysed and verified. The analysis and conclusions can be used as a reference for the investigation of the hydrodynamic performance of wave energy generation devices.

5. Conclusions

In this study, the hydrodynamic performance and energy conversion characteristics of a new oscillating buoy wave energy converter model are investigated using a numerical pool established based on STAR CCM+. Additionally, theoretical analysis and numerical simulation techniques are utilised to study the motion response, force, and output power of the device in a wave environment with four different time periods T and four different wave heights H. Based on the analysis of the calculation results, the following conclusions can be drawn:

(1) In this study, overlapping grid technology is used to numerically simulate the hydrodynamic performance of a power generation device with a wave period T in the range of 1–2.5 s and wave height H in the range of 0.1–0.2 m. Furthermore, the hydrodynamic performance of the device and feasibility of power generation are analysed and verified. Additionally, the numerical simulation calculation can capture the complex flow field information of the device and regularly respond to the change pattern of the device. This can be used as an important tool for the CFD analysis of the new oscillating float-type wave energy generation device.

(2) Under different periods, when $T = 1.5$ s, the device droop velocity amplitude is higher, and the velocity is 0.15 m/s. When $T = 1$ s, the minimum amplitude of the vertical displacement of the device is approximately 0.027 m, but the maximum instantaneous output power is 0.122 W. This is due to the fact that as the wavelength increases, the non-linear effect owing to the change in wave height and water depth is reduced. Therefore, an appropriate adjustment of the wave period is conducive to increasing the output power of the device. However, in actual engineering, the period cannot be reduced indefinitely. This can cause the power generation device to vibrate too fast and can easily cause energy shock and waste. Additionally, the working performance of the related supporting power generation system faces a significant challenge.

(3) Under different wave heights, when wave height $H = 0.15$ m, the device and wave motion amplitude are the most compatible, and the dimensionless T reaches 0.693. When $H = 0.2$ m, the device exhibits the fastest dip motion, and in this case, the turbofan rotates at the fastest speed of 6.67 rad/s and output power is also the highest at 0.211 W. Given that the nonlinear effect due to the change in wave steepness increases when the wavelength is fixed, the appropriate adjustment of the wave height can aid in increasing the output power of the device. However, in actual engineering, the wave height cannot be increased indefinitely as it will lead to the extremely steep waves and upwelling.

Acknowledgments

This study was financially supported by the National Natural Science Foundation of China (51509114) and Jiangsu Basic Research Program (NSFC) (BK2012696, BK2009722).

REFERENCES

[1] Ahn, S., Neary, V. S., Haas, K. A., 2022. Global wave energy resource classification system for regional energy planning and project development. *Renewable and Sustainable Energy Reviews*, 162, 112438. https://doi.org/10.1016/j.rser.2022.112438

[2] Huang, Y., 2020. Research on Key Technologies of Wave Energy Power Generation System. *IOP Conference Series: Earth and Environmental Science*, 585, 012004. https://doi.org/10.1088/1755-1315/585/1/012004

[3] Lu, Z., Shang, J., Luo, Z., Sun, C., Chen, G., 2018. Research on Efficiency of a Wave Energy Conversion System. *IOP Conference Series: Materials Science and Engineering*, 307, 012009. https://doi.org/10.1088/1757-899x/307/1/012009

[4] Ahn, S., Haas, K. A., Neary, V. S., 2020. Wave energy resource characterization and assessment for coastal waters of the United States. *Applied Energy*, 267, 114922. https://doi.org/10.1016/j.apenergy.2020.114922

[5] Kim, S.S., Lee, J.H., Lee, S.S., Kang, D., Lee, S. J., 2018. A Study of Motion Characteristics Led by Connection Methods and Positions of a Wave-Energy Converter in a Regular Wave. *Brodogradnja*, 69(2), 35-54. https://doi.org/10.21278/brod69203

[6] Schubert, B. W., Sergiienko, N. Y., Cazzolato, B. S., Robertson, W. S. P., Ghayesh, M. H., 2022. The true potential of nonlinear stiffness for point absorbing wave energy converters. *Ocean Engineering*, 245, 110342. https://doi.org/10.1016/j.oceaneng.2021.110342

[7] Li, Q., Mi, J., Li, X., Chen, S., Jiang, B., Zuo, L., 2021. A self-floating oscillating surge wave energy converter. *Energy*, 230, 120668. https://doi.org/10.1016/j.energy.2021.120668

[8] Nielsen K, Smed P. F., 1998. Point absorber - Optimization and survival testing.

[9] Weber J, Mouwen F, Parish A, Robertson D., 2009. Wavebob–research & development network and tools in the context of systems engineering.

[10] Chen, W., Dolguntseva, I., Savin, A., Zhang, Y., Li, W., Svensson, O., Leijon, M., 2017. Numerical modelling of a point-absorbing wave energy converter in irregular and extreme waves. *Applied Ocean Research*, 63, 90-105. https://doi.org/10.1016/j.apor.2017.01.004

[11] Kotb, A. T. M., Nawar, M. A. A., Abd El Maksoud, R. M., Mohamed, M. H., 2021. Comprehensive and synergistic analysis of geometry effect on an axial turbine performance for wave energy conversion. *Ocean Engineering*, 233, 109212. https://doi.org/10.1016/j.oceaneng.2021.109212

[12] Takao, M., Setoguchi, T., Kinoue, Y., Kaneko, K., 2006. Effect of end plates on the performence of a wells turbine for wave energy conversion. *Journal of Thermal Science*, 15(4), 319-323. https://doi.org/10.1007/s11630-006-0319-9

[13] Setoguchi, T., & Takao, M., 2006. Current status of self rectifying air turbines for wave energy conversion. *Energy Conversion and Management*, 47(15-16), 2382-2396. https://doi.org/10.1016/j.enconman.2005.11.013

[14] Hashem, I., Abdel Hameed, H. S., Mohamed, M. H., 2018. An axial turbine in an innovative oscillating water column (OWC) device for sea-wave energy conversion. *Ocean Engineering*, 164, 536-562. https://doi.org/10.1016/j.oceaneng.2018.06.067.

[15] Adam, B., Noel, Abderrazak, Abdaoui, & Tarek, et al,2017. Structural health monitoring using wireless sensor networks: a comprehensive survey. IEEE Communications Surveys & Tutorials, 19(3), 1403-1423. https://doi.org/10.1109/COMST.2017.2691551

[16] Miquel, A., Kamath, A., Alagan Chella, M., Archetti, R., Bihs, H., 2018. Analysis of Different Methods for Wave Generation and Absorption in a CFD-Based Numerical Wave Tank. *Journal of Marine Science and Engineering*, 6(2), 73. https://doi.org/10.3390/jmse6020073

[17] Wang, X. S., Wang, L. H., Song, X. F., Ning, B., 2013. 3D Wave Simulation Basing on VOF Method and Dynamic Grid Technology. *Advanced Materials Research*, 774-776, 344-346. https://doi.org/10.4028/www.scientific.net/AMR.774-776.344

[18] Dai, K., Li, Y., Gong, J., Fu, Z., Li, A., Zhang, D., 2022. Numerical Study on Propulsive Factors in Regular Head and Oblique Waves. *Brodogradnja*, 73(1), 37-56. https://doi.org/10.21278/brod73103

[19] Farkas, A., Degiuli, N., Martic, I., 2017. Numerical Simulation of the Viscous Flow Around a Tanker Model. *Brodogradnja*, *68*(2), 109-125. https://doi.org/10.21278/brod68208

[20] Belhenniche, S. E., Aounallah, M., Omar, I., Çelik, F., 2016. Effect Of Geometric Configurations on Hydrodynamic Performance Assessment of a Marine Propeller. *Brodogradnja*, 67(4), 31-48. https://doi.org/10.21278/brod67403

[21] Di Wang, 2019. Numerical Study on Hydrodynamic Performance of Oscillating Float Wave Power Generation Device [D]. *Shanghai Jiao Tong University*. https://doi.org/10.27307/d.cnki.gsjtu.2019.000765

[22] Di Wang, Decheng Wan, 2019. Numerical Simulation of Motion Response of Horizontal Cylindrical Point Suction Wave Power Generation Device [J]. *Hydrodynamic Research and Progress (Part A), 34 (02): 149-158.* https://doi.org/10.16076/j.cnki.cjhd.2019.02.002

[23] Milani, F., Moghaddam, R. K., 2017. Power maximization of a point absorber wave energy converter using improved model predictive control. *China Ocean Engineering*, 31(4), 510-516. https://doi.org/10.1007/s13344-017-0059-5

[24] Yang, S., Wang, Y., He, H., Zhang, J., Chen, H., 2018. Dynamic Properties and Energy Conversion Efficiency of a Floating Multi-Body Wave Energy Converter. *China Ocean Engineering*, 32(3), 347-357. https://doi.org/10.1007/s13344-018-0036-7

[25] Hantoro, R., Septyaningrum, E., Hudaya, Y. R., Utama, I. K. A. P., 2022. Stability Analysis for Trimaran Pontoon Array in Wave Energy Converter – Pendulum System (Wec - Ps). *Brodogradnja*, 73(3), 59-68. https://doi.org/10.21278/brod73304

[26] Zhao, A., Wu, W., Sun, Z., Zhu, L., Lu, K., Chung, H., Blaabjerg, F., 2019. A Flower Pollination Method Based Global Maximum Power Point Tracking Strategy for Point-Absorbing Type Wave Energy Converters. *Energies*, 12(7), 1343. https://doi.org/10.3390/en12071343

[27] Feng, P., Fan, S., Nie, J., Liu, X., 2017. The influence of wave surge force on surf-riding/broaching vulnerability criteria check. *Journal of Hydrodynamics*, 29(4), 596-602. https://doi.org/10.1016/s1001-6058(16)60772-2

Submitted: 27.09.2022.
Accepted: 02.02.2023.

Yu Zhang 1329442491@qq.com
School of Naval Architecture and Ocean Engineering，Jiangsu University of Science and Technology，Zhenjiang 212100，China
Dongqin Li 2947923761@qq.com
School of Naval Architecture and Ocean Engineering，Jiangsu University of Science and Technology，Zhenjiang 212100，China
Shihuan Hong 2201491603@qq.com
School of Chemistry and Chemical Engineering, Jiangsu University，Zhenjiang 212013，China
Miao Zhang 1536193587@qq.com
School of Foreign Languages, Shenyang Jianzhu University，Shenyang 110168，China